Supplement of Atmos. Chem. Phys., 25, 10559–10586, 2025
https://doi.org/10.5194/acp-25-10559-2025-supplement

Atmospheric Chemistry and Physics
Open Access

Supplement of

The influence of ammonia emission inventories on size-resolved global atmospheric aerosol composition and acidity

Xurong Wang et al.

Correspondence to: Alexandra P. Tsimpidi (a.tsimpidi@fz-juelich.de) and Vlassis A. Karydis (v.karydis@fz-juelich.de)

Table S1. Regional NO_x and SO_2 emission amount (Tg yr^{-1}) comparison between CAMS and CEDS_GBD.

	NO_x			SO_2		
	CAMS	CEDS_GBD	Relative difference	CAMS_GBD	CEDS_GBD	Relative difference
Land	75.9	86.2	14%	101.3	104.4	3.1%
North America	8.6	9.2	6.5%	9.6	6.9	-28%
South America	5.4	5.6	2.3%	4.8	5.8	21%
Europe	6.2	7.0	14%	7.9	8.1	2.2%
Middle East	3.3	3.4	3.2%	5.2	6.0	15%
South Asia	6.3	7.0	12%	9.9	9.6	-3.3%
East Asia	17.2	19.0	11%	28.0	29.1	4.0%

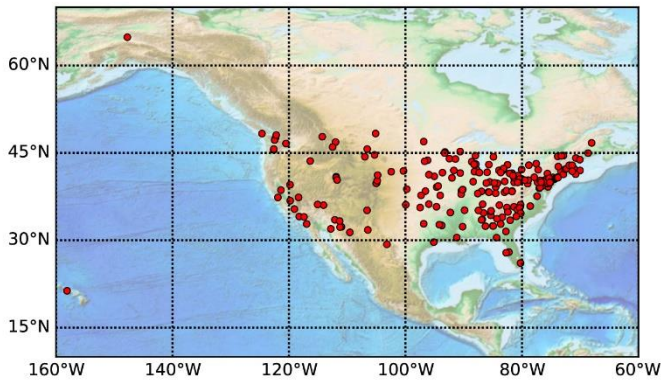

Figure S1. The location of EPA sites represented by red circles.

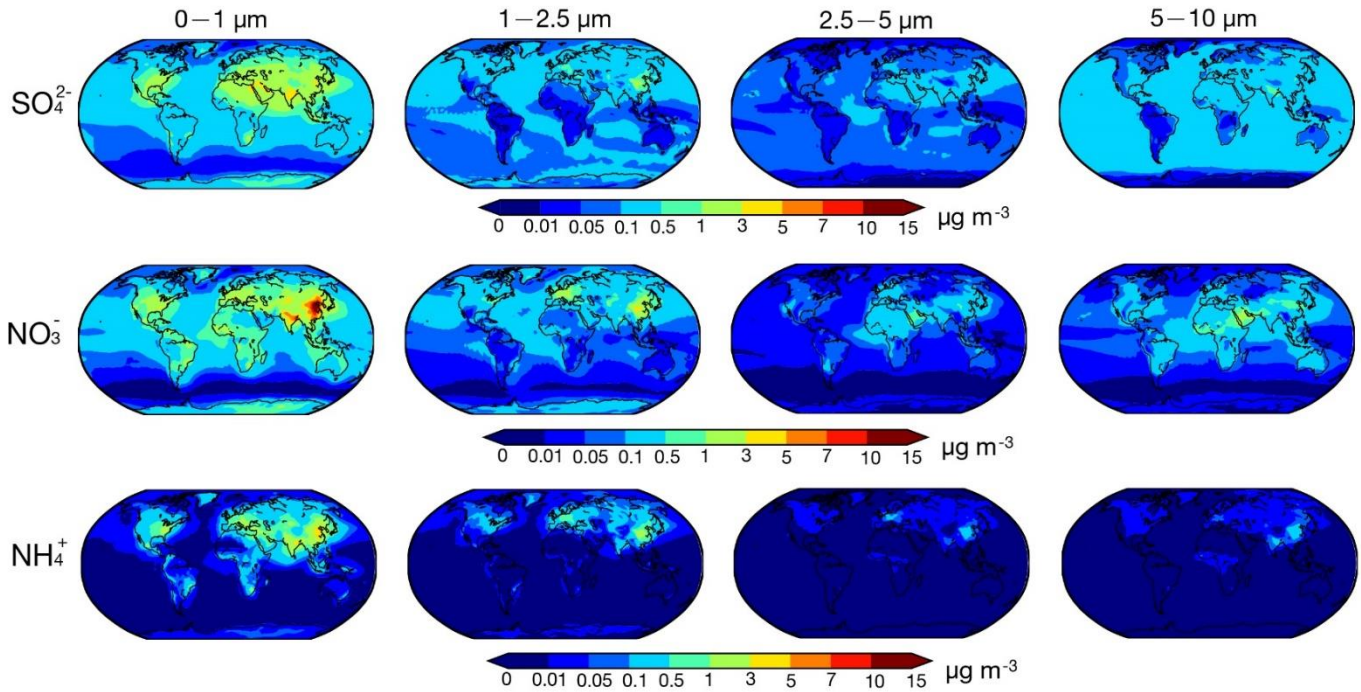

Figure S2. Global distribution maps of SO_4^{2-}, NO_3^-, and NH_4^+ mass concentrations in the size ranges of 0 – 1 μm, 1 – 2.5 μm, 2.5 – 5 μm, and 5 – 10 μm derived from base case simulation, averaged from 2010 to 2012.

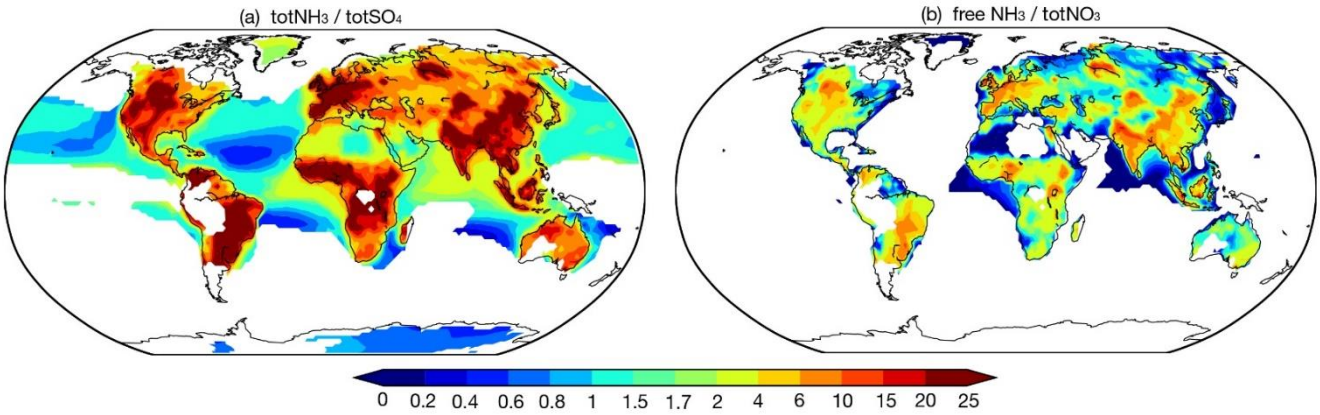

Figure S3. (a) Global distribution molar ratio of $totNH_3$ (sum of NH_4^+ and NH_3) to $totSO_4$ (sum of SO_4^{2-} and HSO_4^-). (b) global distribution molar ratio of free NH_3 ($totNH_3$ minus double $totSO_4$) to $totNO_3$ (sum of NO_3^- and HNO_3), both (a) and (b) are based on SNA molar concentrations in PM_{10} with a threshold of ≥1 μg m^{-3}.

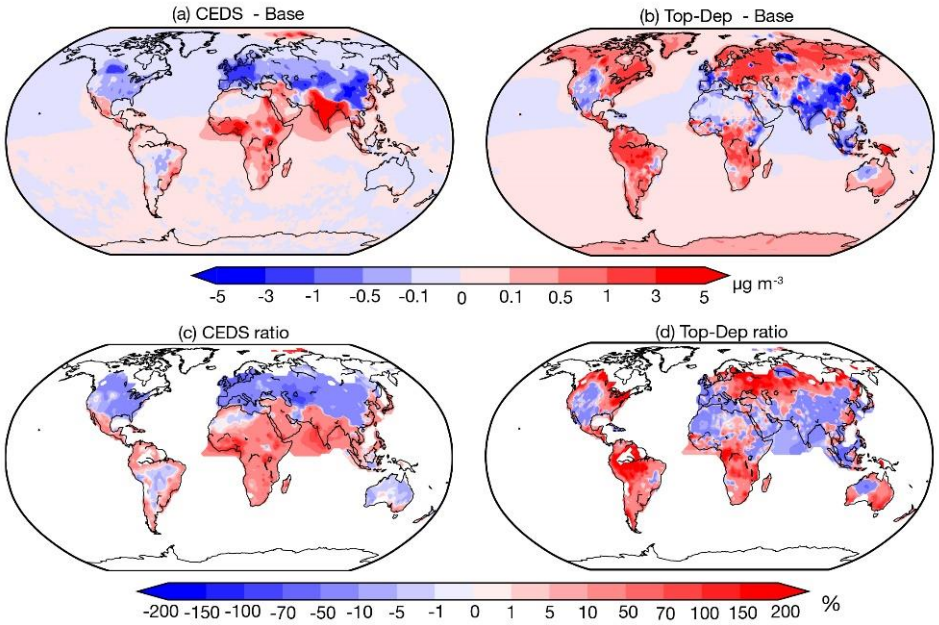

Figure S4. Global distribution maps of surface NH_3 mass concentration absolute difference between CEDS case (a) and Top-Dep case (b) and base case; change ratio (absolute difference/Base case) between CEDS case (c) and Top-Dep case (d) and base case, averaged from 2010 to 2012. The calculation of change ratio is based on the mask of 0.3 μg m^{-3}.

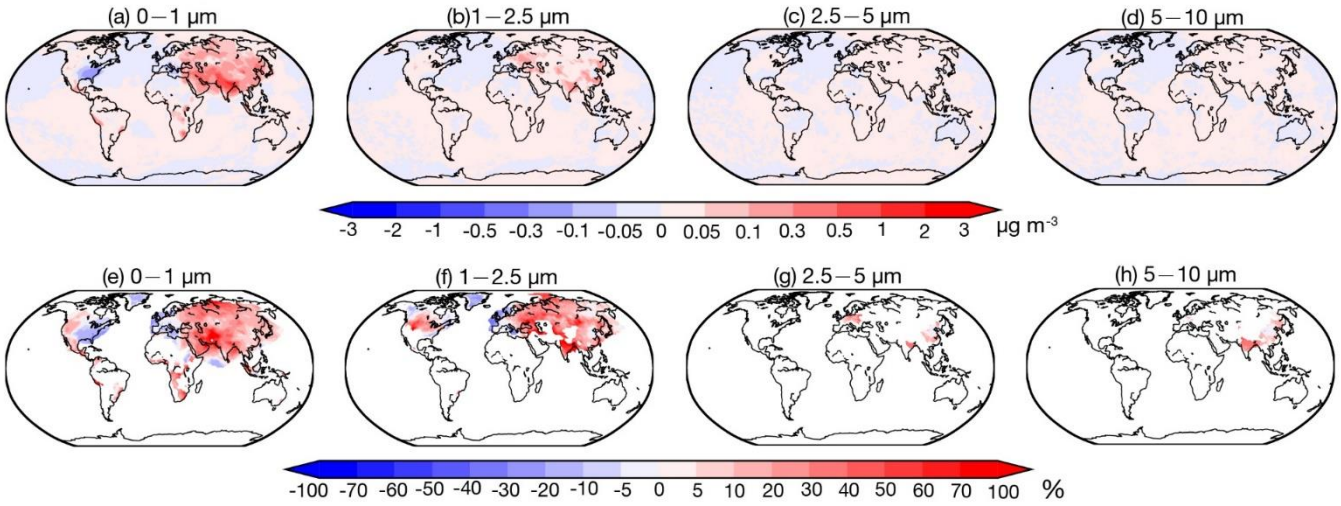

Figure S5. Global distribution maps of surface NH_4^+ mass concentration absolute difference between CEDS case and base case in 0 – 1 μm (a), 1 – 2.5 μm (b), 2.5 – 5 μm (c), 5 – 10 μm (d); change ratio (absolute difference/base case) between CEDS case and base case in 0 – 1 μm (e), 1 – 2.5 μm (f), 2.5 – 5 μm (g), 5 – 10 μm (h), averaged from 2010 to 2012. The calculation of change ratio in full size and 0 – 1 μm is based on the mask of 0.1 μg m^{-3}, in 1 – 2.5 μm, 2.5 – 5 μm and 5 – 10 μm is based on the mask of 0.05 μg m^{-3}.

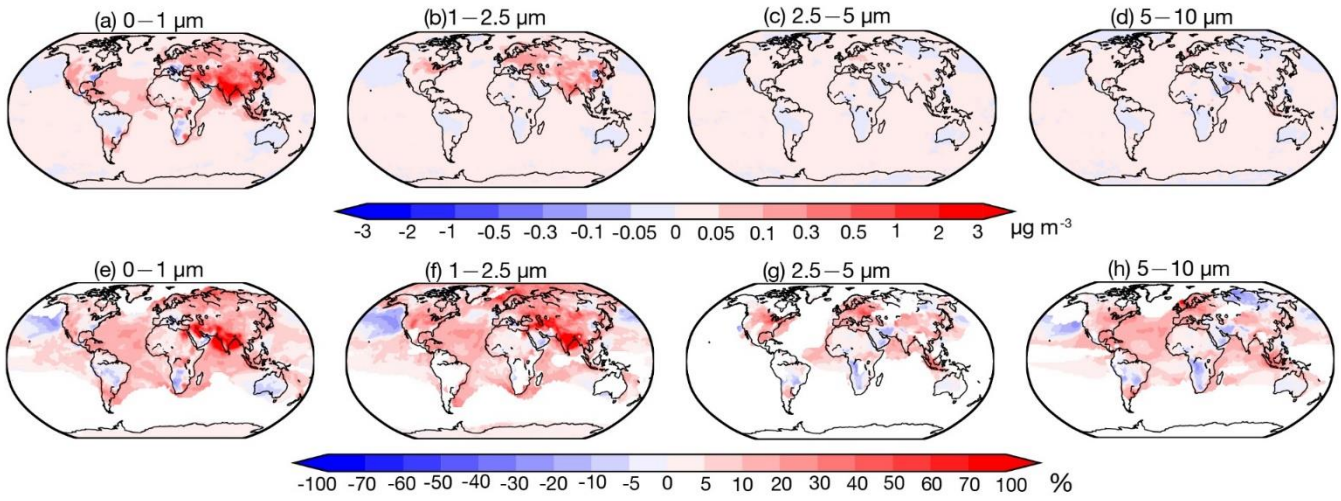

Figure S6. Global distribution maps of surface NO_3^- mass concentration absolute difference between CEDS case and base case in 0 – 1 μm (a), 1 – 2.5 μm (b), 2.5 – 5 μm (c), 5 – 10 μm (d); change ratio (absolute difference/base case) between CEDS case and base case in 0 – 1 μm (e), 1 – 2.5 μm (f), 2.5 – 5 μm (g), 5 – 10 μm (h), averaged from 2010 to 2012. The calculation of change ratio in full size and 0 – 1 μm is based on the mask of 0.1 μg m^{-3}, in 1 – 2.5 μm, 2.5 – 5 μm and 5 – 10 μm is based on the mask of 0.05 μg m^{-3}.

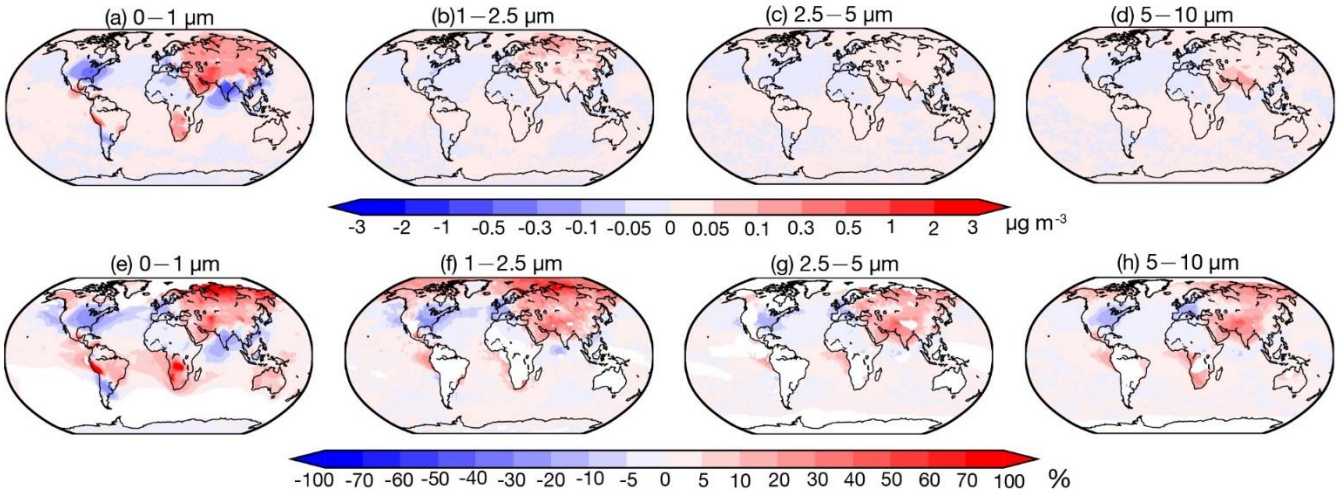

Figure S7. Global distribution maps of surface SO_4^{2-} mass concentration absolute difference between CEDS case and base case in 0 – 1 μm (a), 1 – 2.5 μm (b), 2.5 – 5 μm (c), 5 – 10 μm (d); change ratio (absolute difference/base case) between CEDS case and base case in 0 – 1 μm (e), 1 – 2.5 μm (f), 2.5 – 5 μm (g), 5 – 10 μm (h), averaged from 2010 to 2012. The calculation of change ratio in full size and 0 – 1 μm is based on the mask of 0.1 μg m^{-3}, in 1 – 2.5 μm, 2.5 – 5 μm and 5 – 10 μm is based on the mask of 0.05 μg m^{-3}.

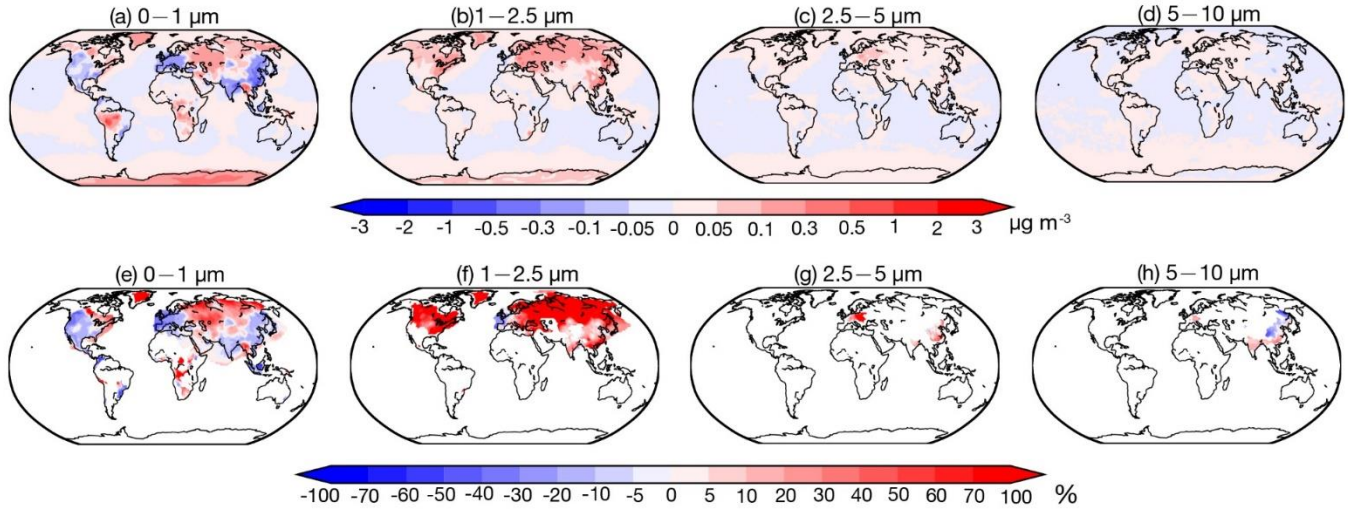

Figure S8. Global distribution maps of surface NH_4^+ mass concentration absolute difference between Top-Dep case and base case in 0 – 1 μm (a), 1 – 2.5 μm (b), 2.5 – 5 μm (c), 5 – 10 μm (d); change ratio (absolute difference/base case) between CEDS case and base case in 0 – 1 μm (e), 1 – 2.5 μm (f), 2.5 – 5 μm (g), 5 – 10 μm (h), averaged from 2010 to 2012. The calculation of change ratio in full size and 0 – 1 μm is based on the mask of 0.1 μg m^{-3}, in 1 – 2.5 μm, 2.5 – 5 μm and 5 – 10 μm is based on the mask of 0.05 μg m^{-3}.

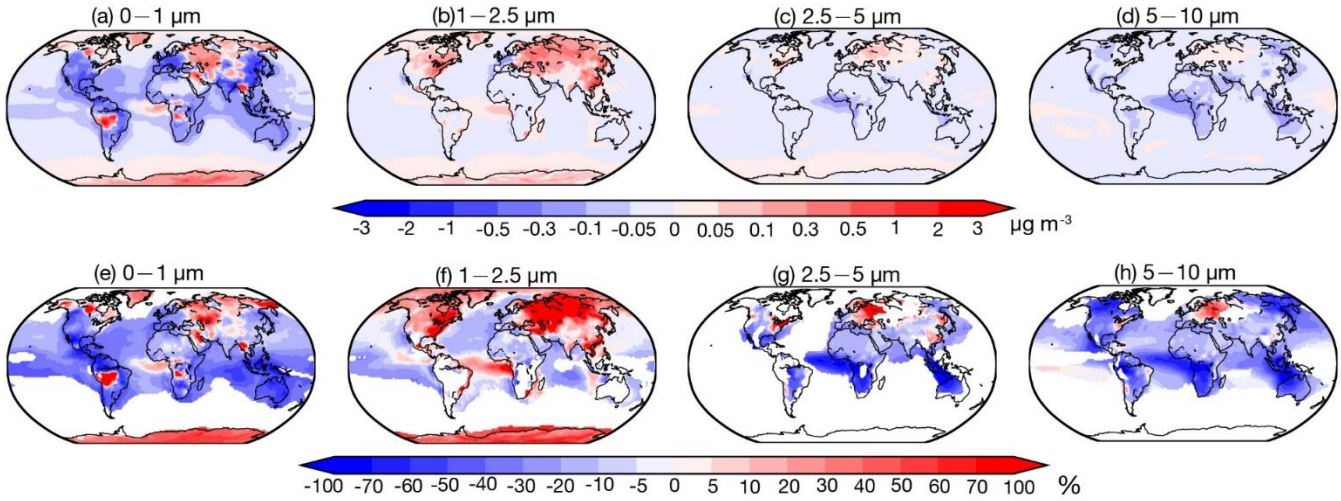

Figure S9. Global distribution maps of surface NO_3^- mass concentration absolute difference between Top-Dep case and base case in 0 – 1 μm (a), 1 – 2.5 μm (b), 2.5 – 5 μm (c), 5 – 10 μm (d); change ratio (absolute difference/base case) between CEDS case and base case in 0 – 1 μm (e), 1 – 2.5 μm (f), 2.5 – 5 μm (g), 5 – 10 μm (h), averaged from 2010 to 2012. The calculation of change ratio in full size and 0 – 1 μm is based on the mask of 0.1 μg m^{-3}, in 1 – 2.5 μm, 2.5 – 5 μm and 5 – 10 μm is based on the mask of 0.05 μg m^{-3}.

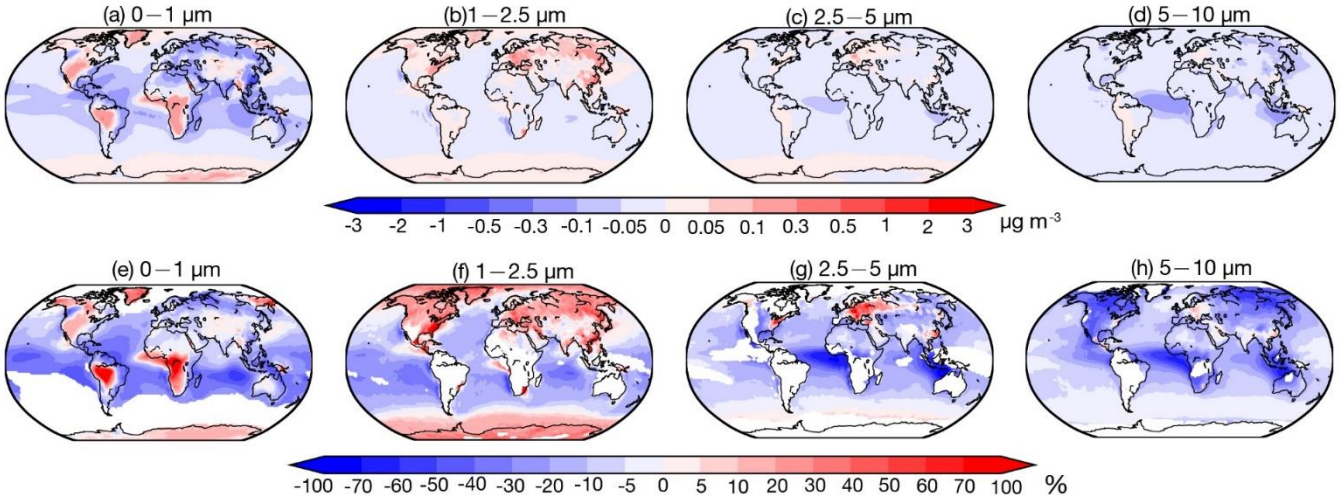

Figure S10. Global distribution maps of surface SO_4^{2-} mass concentration absolute difference between Top-Dep case and base case in 0 – 1 μm (a), 1 – 2.5 μm (b), 2.5 – 5 μm (c), 5 – 10 μm (d); change ratio (absolute difference/base case) between CEDS case and base case in 0 – 1 μm (e), 1 – 2.5 μm (f), 2.5 – 5 μm (g), 5 – 10 μm (h), averaged from 2010 to 2012. The calculation of change ratio in full size and 0 – 1 μm is based on the mask of 0.1 μg m^{-3}, in 1 – 2.5 μm, 2.5 – 5 μm and 5 – 10 μm is based on the mask of 0.05 μg m^{-3}.

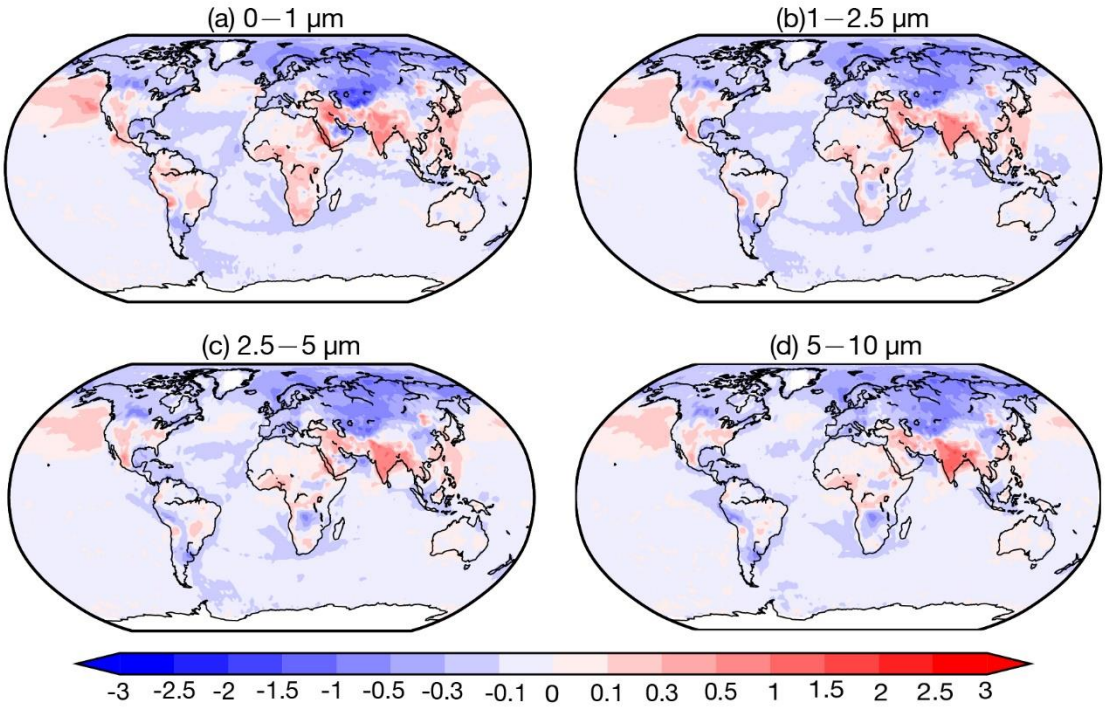

Figure S11. Global distribution maps of pH value absolute difference between CEDS case and base case in the size ranges of 0 – 1 μm, 1 – 2.5 μm, 2.5 – 5 μm, and 5 – 10 μm, averaged from 2010 to 2012.

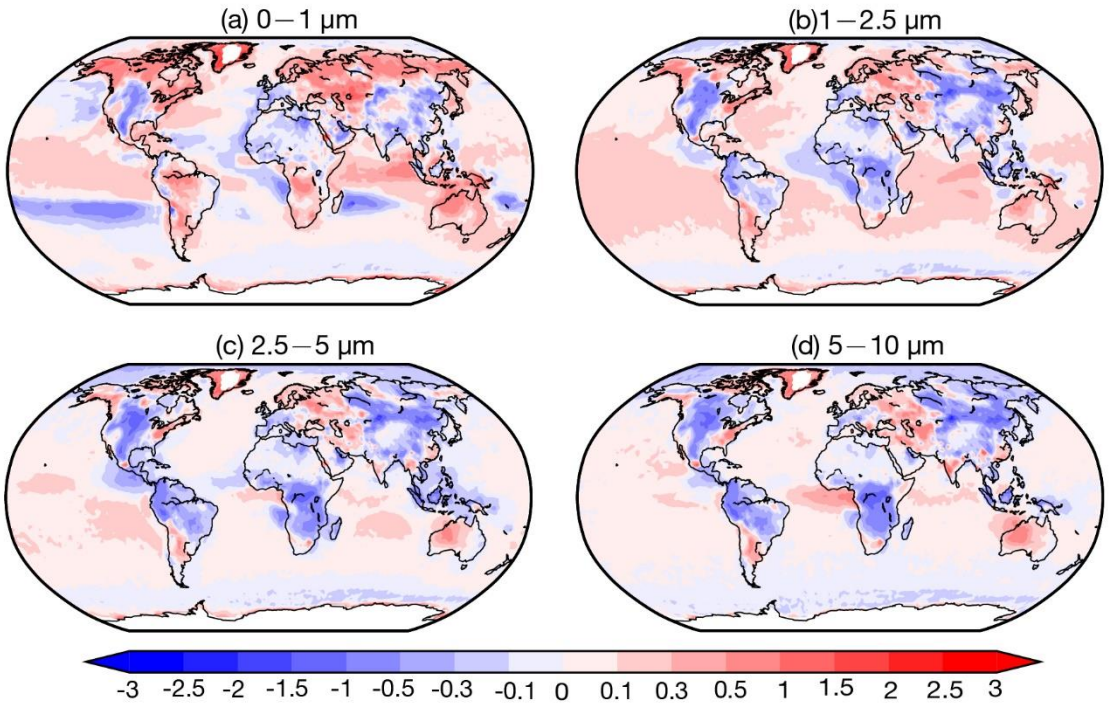

Figure S12. Global distribution maps of pH value absolute difference between Top-Dep case and base case in the size ranges of 0 – 1 μm, 1 – 2.5 μm, 2.5 – 5 μm, and 5 – 10 μm, averaged from 2010 to 2012.

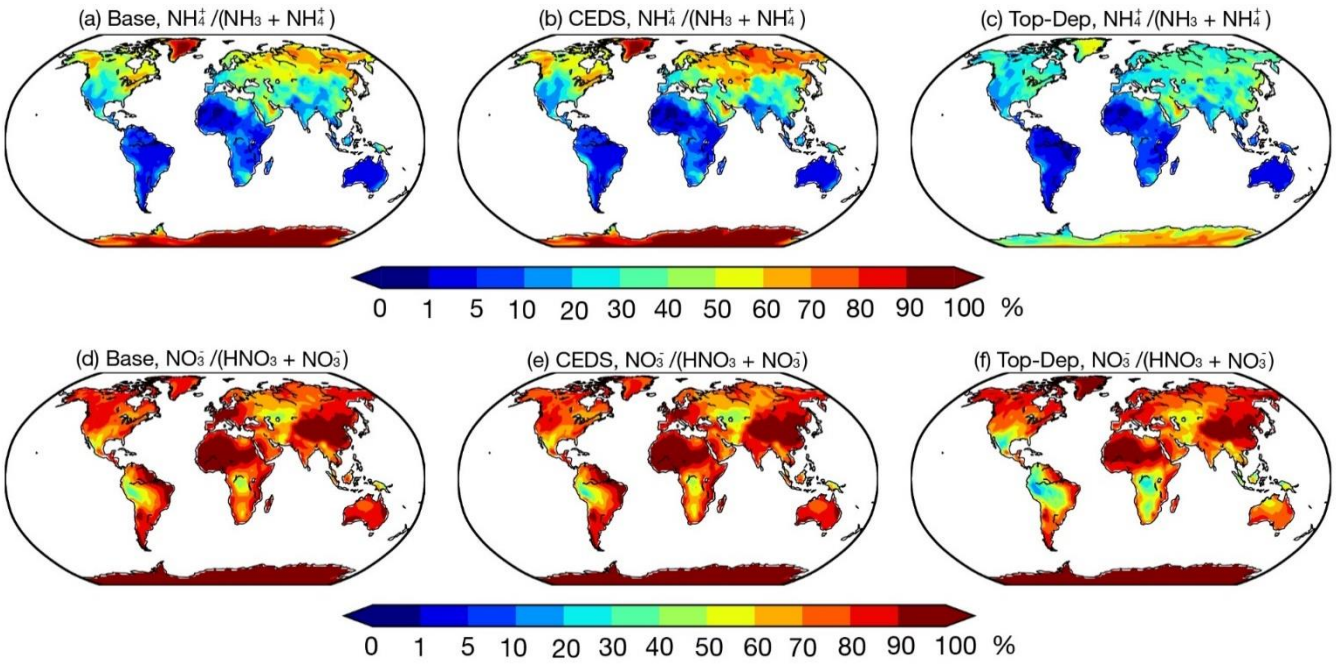

Figure S13. Global distribution maps of gas-particle partitioning molar ratio of NH_3/NH_4^+ and NO_3^-/HNO_3 from simulation results, averaged from 2010 to 2012.

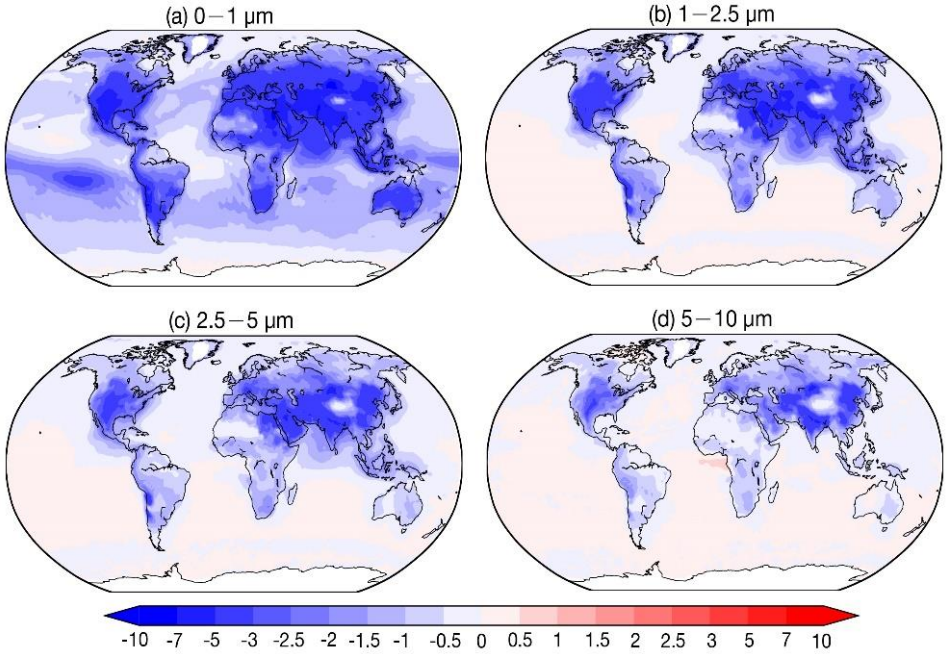

Figure S14. Global distribution maps of pH value absolute difference between noNH_3 case and base case in the size ranges of 0 – 1 μm, 1 – 2.5 μm, 2.5 – 5 μm, and 5 – 10 μm, averaged from 2010 to 2012.

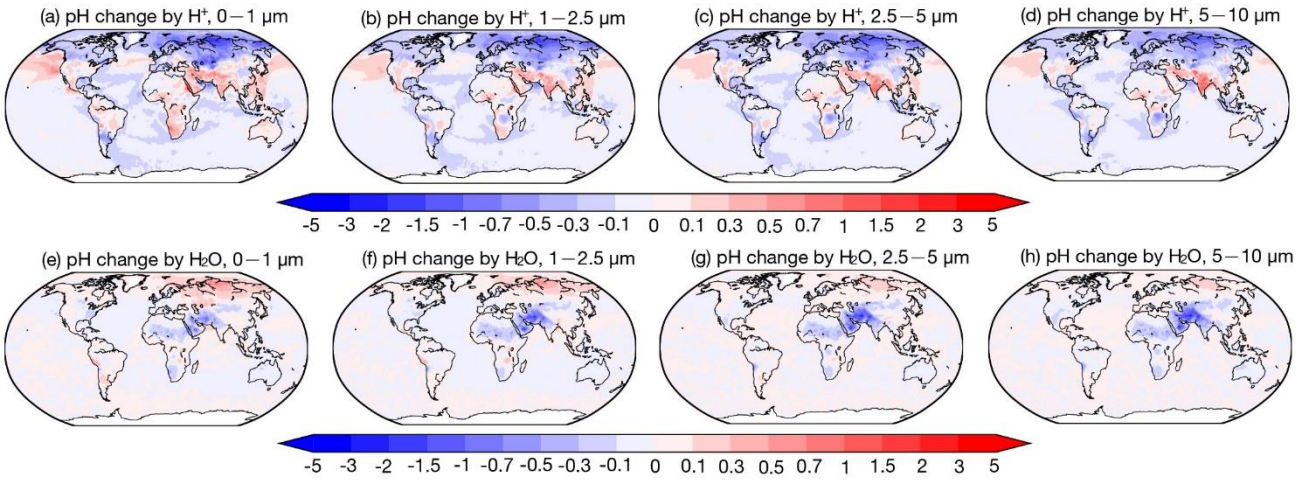

Figure S15. Global distribution of pH value changes derived by H^+ concentration change from CEDS case in the size range of 0 – 1 μm (a), 1– 2.5 μm (b), 2.5 – 5 μm (c), and 5 – 10 μm (d); pH value changes derived by H_2O concentration change in the size range of 0 – 1 μm (e), 1 – 2.5 μm (f), 2.5 – 5 μm (g), and 5 – 10 μm (h), averaged from 2010 to 2012.

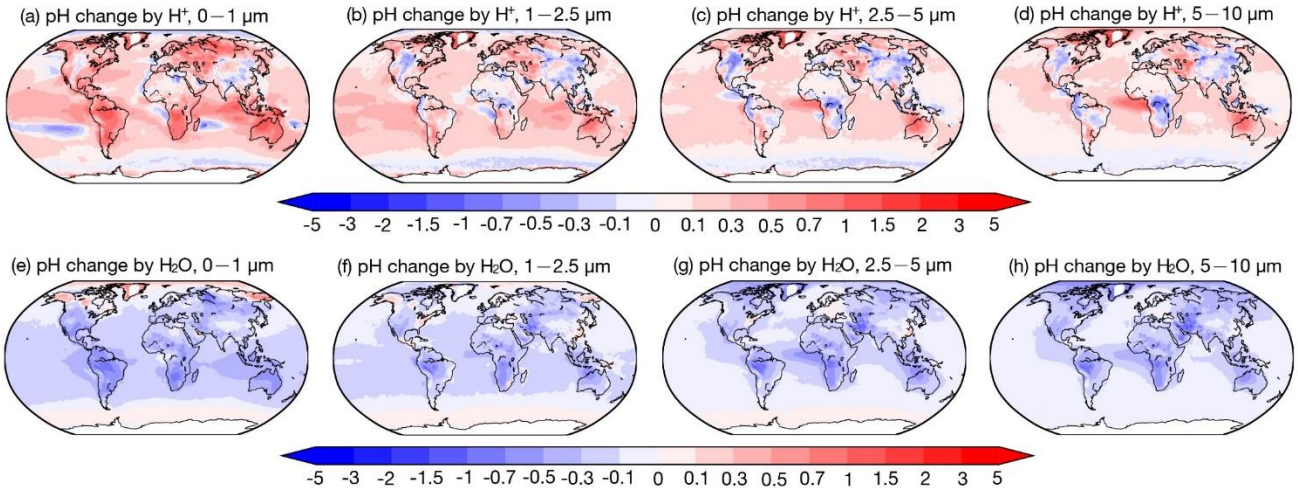

Figure S16. Global distribution of pH value changes derived by H^+ concentration change from Top-Dep case in the size range of 0 – 1 μm (a), 1 – 2.5 μm (b), 2.5 – 5 μm (c), and 5 – 10 μm (d); pH value changes derived by H_2O concentration change in the size range of 0 – 1 μm (e), 1 – 2.5 μm (f), 2.5 – 5 μm (g), and 5 – 10 μm (h), averaged from 2010 to 2012.